JLAB USER GROUP

Jefferson Lab PAC13
Proposal Cover Sheet

This document must be received by close of business Thursday, December 18, 1997 at:

Jefferson Lab
User Liaison Office,
Mail Stop 12B
12000 Jefferson Avenue
Newport News, VA
23606

Experimental Hall: A

Days Requested for Approval: 22

☒ New Proposal Title: STUDY OF THE REACTION $^2H(\vec{e},e'\vec{p})n$ IN THE Δ REGION

☐ Update Experiment Number:

☐ Letter-of-Intent Title:

(Choose one)

Proposal Physics Goals

Indicate any experiments that have physics goals similar to those in your proposal.

Approved, Conditionally Approved, and/or Deferred Experiment(s) or proposals:

NA

Contact Person

Name: ZILU ZHOU
Institution: MIT
Address: Room 26-452, MIT-LNS
Address: 77 MASSACHUSETTS AVE
City, State, ZIP/Country: CAMBRIDGE, MA 02139
Phone: 617-253-5875 Fax: 617-258-5440
E-Mail: ZZHOU@MITLNS.MIT.EDU

JLab Use Only

Receipt Date: 12/18/97 PR97-109

By: gp

BEAM REQUIREMENTS LIST

JLab Proposal No.: _____ Date: 12/18/97

Hall: A Anticipated Run Date: _____ PAC Approved Days: _____

Spokesperson: ZILU ZHOU / WILLIAM BERTOZZI Hall Liaison: KEES DE JAGER
Phone: 617-253-5875
E-mail: ZZHOU@MITLNS.MIT.EDU

List all combinations of anticipated targets and beam conditions required to execute the experiment. (This list will form the primary basis for the Radiation Safety Assesment Document (RSAD) calculations that must be performed for each experiment.)

Condition No.	Beam Energy (MeV)	Mean Beam Current (μA)	Polarization and Other Special Requirements (e.g., time structure)	Target Material (use multiple rows for complex targets — e.g., w/windows)	Material Thickness (mg/cm²)	Est. Beam-On Time for Cond. No. (hours)
1	1645	50	≥40% POL., CW	LD_2	2490	528

The beam energies, E_{Beam}, available are: $E_{Beam} = N \times E_{Linac}$ where N = 1, 2, 3, 4, or 5. E_{Linac} = 800 MeV, i.e., available E_{Beam} are 800, 1600, 2400, 3200, and 4000 MeV. Other energies should be arranged with the Hall Leader before listing.

HAZARD IDENTIFICATION CHECKLIST

JLab Proposal No.: _____ Date: 12/18/97
(For CEBAF User Liaison Office use only.)

Check all items for which there is an anticipated need.

Cryogenics
- _____ beamline magnets
- _____ analysis magnets
- X target
  - type: D_2
  - flow rate: STANDARD
  - capacity: _____

Electrical Equipment
- _____ cryo/electrical devices
- _____ capacitor banks
- _____ high voltage
- _____ exposed equipment

HALL A - STANDARD

Radioactive/Hazardous Materials
List any radioactive or hazadorous/ toxic materials planned for use:

STANDARD

Pressure Vessels
- _____ inside diameter
- _____ operating pressure
- _____ window material
- _____ window thickness

STANDARD

Flammable Gas or Liquids
- type: HALL A
- flow rate: _____
- capacity: STANDARD

Drift Chambers
- type: FPP + VDC
- flow rate: STANDARD
- capacity: _____

Other Target Materials
- ___ Beryllium (Be)
- ___ Lithium (Li)
- ___ Mercury (Hg)
- ___ Lead (Pb)
- ___ Tungsten (W)
- ___ Uranium (U)
- ___ Other (list below)

Vacuum Vessels
- _____ inside diameter
- _____ operating pressure
- _____ window material
- _____ window thickness

STANDARD

Radioactive Sources
- _____ permanent installation
- _____ temporary use
- type: _____
- strength: _____

Large Mech. Structure/System
- _____ lifting devices
- _____ motion controllers
- _____ scaffolding or
- _____ elevated platforms

Lasers
- type: _____
- wattage: _____
- class: _____

Installation:
- _____ permanent
- _____ temporary

Use:
- _____ calibration
- _____ alignment

Hazardous Materials
- ____ cyanide plating materials
- ____ scintillation oil (from)
- ____ PCBs
- ____ methane
- ____ TMAE
- ____ TEA
- ____ photographic developers
- ____ other (list below)

General:

Experiment Class:
- X Base Equipment
- _____ Temp. Mod. to Base Equip.
- _____ Permanent Mod. to Base Equipment
- _____ Major New Apparatus

Other: _____

HALL A - STANDARD EQUIPMENT

LAB RESOURCES LIST

JLab Proposal No.: _____ Date 12/18/97
(For JLab ULO use only.)

List below significant resources — both equipment and human — that you are requesting from Jefferson Lab in support of mounting and executing the proposed experiment. Do not include items that will be routinely supplied to all running experiments such as the base equipment for the hall and technical support for routine operation, installation, and maintenance.

Major Installations *(either your equip. or new equip. requested from JLab)*

HALL A - STANDARD

New Support Structures:

Data Acquisition/Reduction

Computing Resources:

STANDARD

New Software:

Major Equipment

Magnets: HALL A - STANDARD EQUIPMENT

Power Supplies:

Targets:

Detectors:

Electronics:

Computer Hardware:

Other:

Other:

Research Proposal to the JLab PAC 13, December, 1997

Study of the Reaction ^{2}H$(\vec{e}, e'\vec{p})$n in the Δ Region

Co-spokesperson:	William Bertozzi	(email: bertozzi@mitlns.mit.edu)
Co-spokesperson(contact):	Zilu Zhou	(email: zzhou@mitlns.mit.edu)

Abstract

We propose to make precise measurements of the $^2\mathrm{H}(\vec{e}, e'\vec{p})n$ reaction at the Δ-kinematics region. We emphasize the measurements of the differential cross-section, helicity-independent polarization p_n^0, and helicity-dependent polarization components p_t' and p_l' at high initial momenta ($P_m \sim 290 - 450$ MeV/c) and high energy transfer over a large range of proton/virtual-photon angles. Six individual structure functions: helicity-dependent $f_{LT'}^{t}$, $f_{LT'}^{l}$, $f_{T'}^{t}$ and $f_{T'}^{l}$, and helicity-independent f_{LT}^{n} and f_{LT} will be separated. In addition, we will determine the combinations $f_L^n + \frac{\rho_T}{\rho_L} f_T^n + \frac{\rho_{TT}}{\rho_L} f_{TT}^n$ and $f_L + \frac{\rho_T}{\rho_L} f_T + \frac{\rho_{TT}}{\rho_L} f_{TT}$. A careful study of the deuteron is fundamentally important to nuclear physics. Measurements of the recoil proton polarizations and consequently the separated structure functions will give us more complete information about the different aspects of the np system and sub-nucleonic degrees of freedom including meson-exchange currents and isobar configurations, and thus provide a stringent test for theoretical calculations.

Exp. No.	Description	Beam Hours	Energy(GeV)	Current(μA)	Duty Factor
	$^2\mathrm{H}(\vec{e}, e'\vec{p})n$	528	1.645	50	CW

G. A. Warren
University of Basel

K. Aniol, M. Epstein, D. Margaziotis
California State University

W. Boeglin, L. Kramer, P. Markowitz, B. Raue
Florida International University

A. Doley, A. J. Sarty
Florida State University

D. Dale, B. Doyle, A. Gasparian, T. Gorringe, W. Korsch, V. Zeps
University of Kentucky

C. Chang, J. Kelly
University of Maryland

D. Barkhuff, W. Bertozzi, Z. Cai, J. Chen, K. Fissum, R. Florizone, H. Gao, J.C. Gao, S. Gilad, S. Kowalski, C. Kunz, N. Liyanage, M. Ruachev, D. Rowntree, A. Skablin, S.B. Soong, B. Zhang, J.G. Zhao, Z.-L. Zhou
MIT

J. Calarco, F. Hersman, M. Holtrop, M. Leuschner
University of New Hampshire

B. Diederich, K. McCormick, P. Ulmer, L. Weinstein
Old Dominion University

R. Gilman, C. Glashausser, S. Malov, J. McIntyre, R. Ransome
Rutgers University

R. Lourie
SUNY Stony Brook

J.-P. Chen, J. Gomez, O. Hanson, C. W. de Jager, M. Kuss, J. LeRose, M. Liang, B. Michaels, S. Nanda, P. Rutt, A. Saha, B. Wojtsekhowski
Jefferson Lab

K. Joo, R. Lindgren
University of Virginia

D. Armstrong, M. Finn, K. Griffieon, M. Jones, C. Perdrisat, G. Rutledge, G. Quemener, K. Wijesooriya
College of William and Mary

1 Introduction

This proposed experiment is designed to employ spin observables for an enhanced investigation of the dynamical features of the deuteron. Measurements of spin-dependent electron scattering have the potential to greatly enhance our understanding of nucleon and nuclear structure. For example, spin observables in elastic, quasi-elastic, and deep-inelastic scattering from polarized deuterium are predicted to provide important information on the effects of D-wave components in the deuteron ground state wave function [1, 2], the largely unknown charge form factor of the neutron [3], and the neutron spin structure functions [4]. This has prompted development of polarized ^{2}H targets for use with internal [5] or external beams [6] and polarimeters for measuring the polarization of recoiling hadrons [7, 8, 9].

One of the principal goals of nuclear physics is the understanding of nuclear structure and of the underlying nucleon-nucleon (NN) interaction. The deuteron, being the simplest multi-body nucleus, certainly represents one of the most attractive candidates for the investigation of the NN interaction. The experimental study of the large momentum behavior of the deuteron wave function is of particular importance for a determination of the short-range properties of the nuclear forces. The continuing interest in the electro-disintegration of deuteron reflects the fact that it provides a very powerful tool to investigate the structure of the two-nucleon system and its electromagnetic properties.

The ^{2}H nucleus has the attractive feature that it can be used as a neutron target. In good approximation it can be considered as a proton-neutron pair. This is exemplified by the deuteron magnetic moment, $\mu_{\rm d} = 0.857\ \mu_{\rm N}$ ($\mu_{\rm N}$ = nuclear magneton), which is approximately equal to the sum of the proton and neutron magnetic moments, $\mu_{\rm p} + \mu_{\rm n} = (2.793 - 1.913)\ \mu_N = 0.880\ \mu_{\rm N}$. Thus, it should be possible to determine the charge and magnetic properties of the neutron from measurements of quasi-elastic electron scattering from ^{2}H. Indeed, it has been suggested [3] that the $^2\vec{\rm H}(\vec{e}, e'n)p$ [$^2{\rm H}(\vec{e}, e'\vec{n})p$] experiment with longitudinally polarized electrons and a vector polarized deuteron target (a recoil neutron polarimeter) can provide data on G_E^n. Such experiments have been conducted or proposed [9, 10, 11].

Therefore, an important question is to what extent the deuteron can be used as a neutron target in order to measure the electromagnetic form-factor of the neutron. Crucial to the extraction of precise information on the neutron using the electron scattering from ^{2}H not only requires a detailed understanding of the deuteron structure, but also needs a quantitative understanding of the reaction mechanism, such as the effects of relativistic corrections (RC), final-state interactions (FSI), meson-exchange currents (MEC) and the isobar excitations (IC), in the kinematic regimes investigated.

Of interest in this respect is the study of interaction effects like the presence of mesonic exchange currents and the influence of internal nucleon degrees of freedom in terms of nuclear isobar configurations. Again these interaction effects can be most clearly studied in the two-nucleon system since one does not need to deal with problems and approximations of many-body systems, which usually make the interpretation of such effects in heavier nuclei less conclusive. For the same reason, the deuteron is often used as a benchmark to

test nuclear theory.

The importance of the meson-exchange currents and isobar contributions can be demonstrated, again, by the static deuteron magnetic moment. The difference between the deuteron magnetic moment and the sum of the proton and neutron magnetic moments cannot be fully attributed to the deuteron D-state probability and relativistic corrections. It is found [13] that the contributions of meson-exchange currents and the isobar components, although small, have to be taken into account.

Careful studies of these effects in the deuteron require selection of the reactions and kinematics. For example, in the *e-d* elastic scattering, the isospin selection rules forbid a single Δ-excitation. In this case, only contributions from higher-order components are possible. This makes the study difficult.

However, the deuteron electro-disintegration in the Δ-resonance region offers an excellent probe with which to investigate the dynamics of the Δ-isobar and pionic exchange in a nuclear system. Although the effects of these mechanisms are small in quasi-elastic kinematics, they are expected to be important at higher excitation energies [14]. Furthermore, in deuteron electro-disintegration, one can judicially choose the kinematics to precisely separate the structure functions. For example, one can separate the cross section into the longitudinal (L), transverse (T), LT and TT interference structure functions. The transverse structure function (and transverse-transverse interference structure function) is generally more sensitive to the meson-exchange and isobar effects, while the longitudinal structure function is (to first order) a measure of the one-body charge distribution. The measurements of those structure functions sensitive to the meson-exchange currents and isobar contributions are a strong test of the theoretical treatment of pionic and Δ degrees of freedom. Such a study is of interest for a proper description of medium effects on the Δ propagation and meson exchange in the deuteron.

Therefore, most of the experimental and theoretical studies of the deuteron electro-disintegration have concentrated on either of these two somewhat opposing aspects depending on the choice of energy and momentum transfer. On the one hand, one intends to choose the kinematic regions where the effects of reaction mechanism are expected to be small and can be neglected. In this approximation one can obtain a simple determination of the nucleon momentum distribution inside the deuteron [15, 16] or the information on the deuteron ground state wave function [17]. In addition, as mentioned above, one can use the deuteron as a neutron/proton target in order to determine the electric and magnetic form factors of the neutron/proton. On the other hand, one can choose kinematics regions where the various interaction effects are enhanced. These effects include the relativistic corrections, the final-state interactions, meson-exchange currents and the isobar contributions. Careful studies of these effects are fundamental to nuclear physics.

2 Status and aim

Presently, many state-of-art calculations for the deuteron electro-disintegration are available in both non-relativistic and fully relativistic approaches (see for example [1, 2, 18, 19, 20, 21, 22]). On the experimental side, many measurements have been performed especially in the past decade. However, data are still limited. Most of the measurements have been done with the unpolarized ^{2}H$(e,e'p)n$ reaction. Furthermore, they were limited to the study of cross section and/or those few unpolarized structure functions. Only recently, due to the development of the recoil polarimetry (and also polarized ^{2}H targets), polarization measurements utilizing the ^{2}H$(\vec{e},e'\vec{p})n$ and ^{2}H$(\vec{e},e'\vec{n})p$ [also $^2\vec{\text{H}}(\vec{e},e')$ and $^2\vec{\text{H}}(\vec{e},e'p)n$] reactions are possible. However, before TJNAF, measurements have been limited to quasi-elastic conditions and to low recoil momenta. With the capabilities of TJNAF one can test state-of-art calculations in more detail by pushing the limits with high energy transfer, studying regimes of high recoil momenta and trying to separate more structure functions especially those which are more sensitive to the interaction effects. Of particular interest, one investigates the expected failure of non-relativistic models

Existing data and proposed measurements on the ^{2}H$(e,e'p)n$ and ^{2}H$(\vec{e},e'\vec{p})n$ have been extensively surveyed and discussed in Ref. [23]. We only briefly bring up the relevant issues here while leaving the detailed discussion to Ref. [23] and references therein.

- Recent measurements [24, 25] of the longitudinal structure function, f_L, yielded results about 20% lower than theory. This discrepancy adds to the controversy of failure of the Coulomb Sum Rule to describe the integrated longitudinal response for nuclei (see for example [26]). More precise measurements are planned at Hall A [27].

- Measurements of the left-right asymmetry, A_{LT}, demonstrate the necessity of including relativistic corrections [24, 25, 28, 29, 30, 31, 32]. However, the separated longitudinal-transverse structure, f_{LT} (which is different from A_{LT}), was better described by the completely non-relativistic model without relativistic corrections [24, 25]. Furthermore, A_{LT} data at Q^2=1.6 (GeV/c)^2 and with the recoil momenta up to 150 MeV/c [30] agreed with a PWIA calculation based on the prescription σ_{cc1} of de Forest [33] for the half-off-shell electron-proton cross section and the Paris spectral function [34].

- Measurements of the transverse-transverse structure function, f_{TT}, have been recently performed in Δ kinematics at NIKHEF, and the data show the domination of the isobar contributions [35]. While f_{TT} data is well reproduced by calculations in the impulse approximation, the cross sections are better reproduced by calculations in a couple-channel framework [22]. This indicate the theoretical understanding is not complete. More precise measurements of f_{TT} together with f_{LT} and f'_{LT} are proposed at MIT-Bates using the out-of-plane spectrometers (OOPS) [36].

- Recent measurements of G_E^n [9, 10] have been performed using a deuterium target and the ^{2}H$(\vec{e},e'\vec{n})p$ reaction. The results from Ref. [10] cause some controversy.

- Measurements of G_E^p using a recoil proton polarimeter have been performed at MIT-Bates with a comparison of $^2H(\vec{e}, e'\vec{p})n$ (quasi-elastic and $p_m = 0$) and $^1H(\vec{e}, e'\vec{p})$ reactions. The results [37] show that in these kinematics the nuclear effects relating to the G_E^p measurements are very small, and that deuterium can serve as a proton and hence also as a neutron target for this purpose. However, it has been indicated that even in quasi-elastic kinematics the calculations describe the measurements better at $p_m = 0$ than at $p_m = 100$ MeV/c [38]. This result suggests for more measurements at higher p_m and at both non-parallel and parallel kinematics. However, these kinematics are not presently accessible at Bates because of low counting rates and low figure of merits [39].

- Further measurements of both G_E^p [40] and G_E^n [11, 12] have been planned at Hall A and Hall C at high momentum transfer. But all measurements will be limited to quasi-elastic kinematics. Furthermore, no precise separation of structure functions will be made. Therefore, the detailed interaction effects have never been studied. Thus, there is a need in making efforts towards understanding of polarization observables in the $^2H(\vec{e}, e'\vec{p})n$ and $^2H(\vec{e}, e'\vec{n})p$ reactions.

It is the aim of this proposed experiment to investigate the disintegration processes $^2H(\vec{e}, e'\vec{p})n$ in the Δ region where the knock-out proton is detected and polarization analyzed in coincidence with the scattered electron. We plan to make precise measurements utilizing the high-resolution spectrometers and the focal-plane polarimeter at Hall A. We emphasize the measurements of the differential cross-section, helicity-independent polarization p_n^0, and helicity-dependent polarization components p_t' and p_l' at high initial momenta ($P_m \sim 290 - 450$ MeV/c) and high energy transfer over a large range of proton/virtual-photon angles. In this way, six individual structure functions: $f_{LT}^{\prime t}$, $f_{LT}^{\prime l}$, f_{LT}^n, f_{LT}, $f_T^{\prime t}$ and $f_T^{\prime l}$ will be separated. In addition, we will determine the combinations $f_L^n + \frac{\rho_T}{\rho_L} f_T^n + \frac{\rho_{TT}}{\rho_L} f_{TT}^n$ and $f_L + \frac{\rho_T}{\rho_L} f_T + \frac{\rho_{TT}}{\rho_L} f_{TT}$. In the Δ kinematics, the polarization observables are predicted to have great sensitivities to the nuclear interaction effects such as the relativistic corrections, final-state interactions, meson-exchange currents and isobar contributions [19].

3 Formalism and expectation

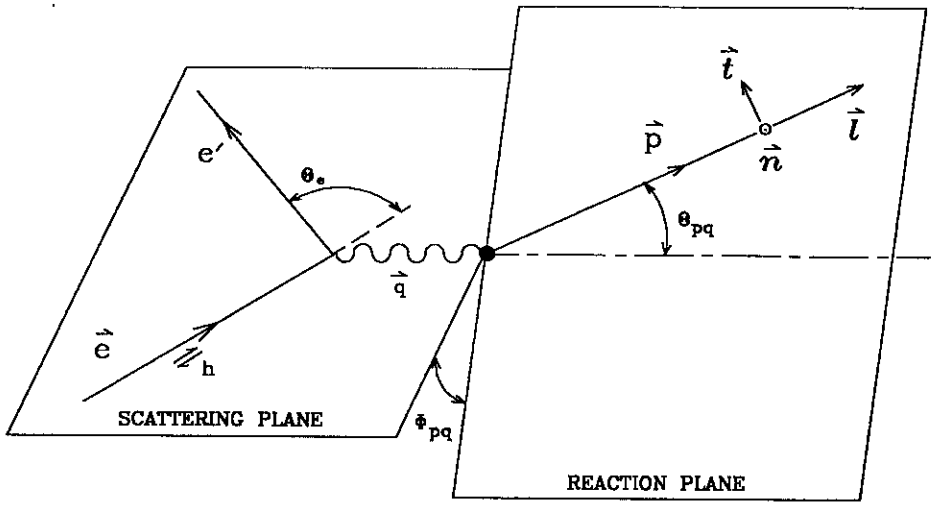

Figure 1: Geometry of exclusive electron scattering with polarized electrons and polarized recoil protons. The components of the polarization of the recoil protons are denoted by (t,n,l). $\vec{l}$ is parallel to $\vec{p}$ and $\vec{n}$ is parallel to $\vec{q}\times\vec{p}$, perpendicular to the reaction plane.

A schematic representation of the $^2\mathrm{H}(\vec{e},e'\vec{p})n$ reaction is presented in Fig. 1. Here, a non-vanishing $\theta_{\mathrm{pq}}^{\mathrm{cm}}$ corresponds to a measurement in "non-parallel kinematics". When $\phi_{\mathrm{pq}}^{\mathrm{cm}}$ is neither 0° nor 180°, the kinematics is called "out of plane". Note that, "cm" refers to the reference frame associated with the final $n-p$ center of mass system. The cross section of the reaction described in Fig. 1 can be written as a sum of terms which include 18 independent structure functions $\mathrm{f_{ij}}$ in the following form [1, 18, 19]

$$
\begin{aligned}
\frac{d\sigma\ (1+\vec{P})}{d\Omega_{e'}^{\mathrm{lab}}de'^{\mathrm{lab}}d\Omega_{\mathrm{pq}}^{\mathrm{cm}}} &= c\Big\{(\rho_{\mathrm{L}}f_{\mathrm{L}}+\rho_{\mathrm{T}}f_{\mathrm{T}}+\rho_{\mathrm{LT}}f_{\mathrm{LT}}\cos\phi_{\mathrm{pq}}^{\mathrm{cm}}+\rho_{\mathrm{TT}}f_{\mathrm{TT}}\cos 2\phi_{\mathrm{pq}}^{\mathrm{cm}}) \\
&\quad +h\,\rho'_{\mathrm{LT}}f'_{\mathrm{LT}}\sin\phi_{\mathrm{pq}}^{\mathrm{cm}} \\
&\quad +(\rho_{\mathrm{L}}f_{\mathrm{L}}^{n}+\rho_{\mathrm{T}}f_{\mathrm{T}}^{n}+\rho_{\mathrm{LT}}f_{\mathrm{LT}}^{n}\cos\phi_{\mathrm{pq}}^{\mathrm{cm}}+\rho_{\mathrm{TT}}f_{\mathrm{TT}}^{n}\cos 2\phi_{\mathrm{pq}}^{\mathrm{cm}}) \\
&\quad +(\rho_{\mathrm{LT}}f_{\mathrm{LT}}^{l}\sin\phi_{\mathrm{pq}}^{\mathrm{cm}}+\rho_{\mathrm{TT}}f_{\mathrm{TT}}^{l}\sin 2\phi_{\mathrm{pq}}^{\mathrm{cm}}) \\
&\quad +(\rho_{\mathrm{LT}}f_{\mathrm{LT}}^{t}\sin\phi_{\mathrm{pq}}^{\mathrm{cm}}+\rho_{\mathrm{TT}}f_{\mathrm{TT}}^{t}\sin 2\phi_{\mathrm{pq}}^{\mathrm{cm}}) \\
&\quad +h\,\rho'_{\mathrm{LT}}f'^{\,n}_{\mathrm{LT}}\sin\phi_{\mathrm{pq}}^{\mathrm{cm}} \\
&\quad +h\,(-\rho'_{\mathrm{T}}f'^{\,l}_{\mathrm{T}}-\rho'_{\mathrm{LT}}f'^{\,l}_{\mathrm{LT}}\cos\phi_{\mathrm{pq}}^{\mathrm{cm}}) \\
&\quad +h\,(-\rho'_{\mathrm{T}}f'^{\,t}_{\mathrm{T}}-\rho'_{\mathrm{LT}}f'^{\,t}_{\mathrm{LT}}\cos\phi_{\mathrm{pq}}^{\mathrm{cm}})\Big\}\,, \\
&= \sigma^{0}_{\phi_{\mathrm{pq}}^{\mathrm{cm}}}\,(1+hA'_{\mathrm{LT}}+p_n^0+p_l^0+p_t^0+hp'_n+hp'_l+hp'_t)\,, \\
&= \sigma^{h}_{\phi_{\mathrm{pq}}^{\mathrm{cm}}}\,(1+\vec{P})\,, \qquad (1)
\end{aligned}
$$

where c is proportional to the Mott cross section, ρ_{ij} are kinematic terms which depend

only on the electron kinematics (q and ω, the momentum and energy transfer), and the $'$ (^{0}) denotes (in-)dependence on the electron helicity. A'_{LT} represents the helicity asymmetry related the term of f'_{LT}, and p's are recoil nucleon polarization components contributed by corresponding structure functions.

For coplanar (in-plane) kinematics where $\phi^{cm}_{pq} = 0°$ or 180°, the polarization independent part of the cross-section and the recoil polarization components reduces to:

$$\sigma^0_{\phi^{cm}_{pq}} = c(\rho_L f_L + \rho_T f_T + \rho_{LT} f_{LT} \cos\phi^{cm}_{pq} + \rho_{TT} f_{TT} \cos 2\phi^{cm}_{pq}) , \quad (2)$$

$$p^0_n = \frac{c}{\sigma^0_{\phi^{cm}_{pq}}} \cdot (\rho_L f^n_L + \rho_T f^n_T + \rho_{LT} f^n_{LT} \cos\phi^{cm}_{pq} + \rho_{TT} f^n_{TT} \cos 2\phi^{cm}_{pq}) , \quad (3)$$

$$p'_l = \frac{c}{\sigma^0_{\phi^{cm}_{pq}}} \cdot (-\rho'_T f'^{\,l}_T - \rho'_{LT} f'^{\,l}_{LT} \cos\phi^{cm}_{pq}) , \quad (4)$$

$$p'_t = \frac{c}{\sigma^0_{\phi^{cm}_{pq}}} (-\rho'_T f'^{\,t}_T - \rho'_{LT} f'^{\,t}_{LT} \cos\phi^{cm}_{pq}) . \quad (5)$$

In addition, one can form left-right asymmetry A_{LT} from the cross section measurements. The asymmetry A_{LT} is related to the structure function f_{LT}:

$$A_{LT} = \frac{\sigma^0_{0°} - \sigma^0_{180°}}{\sigma^0_{0°} + \sigma^0_{180°}} = \frac{\rho_{LT} f_{LT}}{\rho_L f_L + \rho_T f_T + \rho_{TT} f_{TT}} . \quad (6)$$

However, A_{LT} and f_{LT} differ by a denominator so that their physics sensitivity may not be same.

Obviously, in measuring the polarization components and A_{LT}, asymmetries rather than the absolute cross sections play the important role. Hence, issues relating to systematic uncertainties tend to become less significant in determining the quality of the measurements.

If one measures cross sections and polarization components at both $\phi^{cm}_{pq} = 0°$ and 180° sides, then one can extract individual structure functions. In Eq. 7, schemes are shown to measure separated or combined structure functions.

$$\begin{aligned}
f_{LT} &= [\sigma^0_{\phi^{cm}_{pq}=0°} - \sigma^0_{180°}]/(2c\rho_{LT}) , \\
f_L + \frac{\rho_T}{\rho_L} f_T + \frac{\rho_{TT}}{\rho_L} f_{TT} &= [\sigma^0_{0°} + \sigma^0_{180°}]/(2c\rho_L) , \\
f^n_{LT} &= [\sigma^0_{0°} \cdot p^0_n(\phi^{cm}_{pq} = 0°) - \sigma^0_{180°} \cdot p^0_n(180°)]/(2c\rho_{LT}) , \\
f^n_L + \frac{\rho_T}{\rho_L} f^n_T + \frac{\rho_{TT}}{\rho_L} f^n_{TT} &= [\sigma^0_{0°} \cdot p^0_n(0°) + \sigma^0_{180°} \cdot p^0_n(180°)]/(2c\rho_L) , \\
f'^{\,l}_T &= [\sigma^0_{0°} \cdot p'_l(0°) + \sigma^0_{180°} \cdot p'_l(180°)]/(-2c\rho'_T) , \\
f'^{\,l}_{LT} &= [\sigma^0_{0°} \cdot p'_l(0°) - \sigma^0_{180°} \cdot p'_l(180°)]/(-2c\rho'_{LT}) ,
\end{aligned}$$

$$
\begin{aligned}
f'^{t}_{\mathrm{T}} &= [\sigma^0_{0^\circ} \cdot p'_t(0^\circ) + \sigma^0_{180^\circ} \cdot p'_t(180^\circ)]/(-2c\rho'_{\mathrm{T}}) \,, \\
f'^{t}_{\mathrm{LT}} &= [\sigma^0_{0^\circ} \cdot p'_t(0^\circ) - \sigma^0_{180^\circ} \cdot p'_t(180^\circ)]/(-2c\rho'_{\mathrm{LT}}) \,. \qquad (7)
\end{aligned}
$$

In parallel kinematics, where $\theta^{\mathrm{cm}}_{pq} = 0$, the interference structure functions $\mathrm{f_{LT}}$ and $\mathrm{f_{TT}}$ go to zero. Measurements are planned at Bates to extract the structure functions $\mathrm{f'_{LT}}$ and $\mathrm{f_{TT}}$ simultaneously with $\mathrm{f_{LT}}$ by using the out-of-plane spectrometers. One can extract the structure functions $\mathrm{f_L}$ and $\mathrm{f_T}$ by performing a Rosenbluth separation. However, we would like to limit the scope of discussion relevant to this proposal.

It is clear from Eq. 1 and 7 that a complete separation of all 18 available structure functions is very difficult. However, it is also clear that by selecting appropriate kinematics, a measurement of many structure functions is, in principle, straight forward.

The advantage of measuring structure functions is illustrated by the relation of the components of the electromagnetic nuclear current, $\vec{J}$, and those 5 structure functions which do not require the detection of the hadron polarization.

$$
\begin{aligned}
f_{\mathrm{L}} &\equiv f_{00} \quad \propto \quad J^*_0 J_0 \,, \\
f_{\mathrm{T}} &\equiv f_{11} \quad \propto \quad J^*_{+1} J_{+1} + J^*_{-1} J_{-1} \,, \\
f_{\mathrm{TT}} &\equiv f_{1-1} \quad \propto \quad \mathrm{Re}\Big\{ J^*_{+1} J_{-1} \Big\} \,, \\
f_{\mathrm{LT}} &\equiv f_{01} \quad \propto \quad \mathrm{Re}\Big\{ J^*_0 (J_{+1} - J_{-1}) \Big\} \,, \\
f'_{\mathrm{LT}} &\equiv f'_{01} \quad \propto \quad \mathrm{Im}\Big\{ J^*_0 (J_{+1} - J_{-1}) \Big\} \,.
\end{aligned} \qquad (8)
$$

Hence, by measuring the interference structure functions, the smaller component $\mathrm{J_0}$ is amplified by the larger components $\mathrm{J_\pm}$. Similar relations can be written for those structure functions corresponding to the components of recoil polarization. It is evident that measuring more structure functions enables more detailed theoretical understanding of the current.

For those polarization structure functions, only $\mathrm{f^n_{LT}}$, $\mathrm{f'^{t}_{LT}}$ and $\mathrm{f'^{l}_{T}}$ survive in parallel kinematics. Furthermore, in quasi-elastic scattering and with $\mathrm{p_m} = 0$, the two components of polarization p'_t and p'_l in the scattering plane are very nearly the same as for elastic e-p or e-n scattering. These can be written in terms of the elementary nucleon form factors, $\mathrm{G^N_E}$ and $\mathrm{G^N_M}$. Consequently, the ratios of $\mathrm{G^N_E}$ and $\mathrm{G^N_M}$ are related to the ratios of p'_t and p'_l of the ejected nucleon polarization by kinematic factors only [41]:

$$
\frac{G^{\mathrm{N}}_{\mathrm{E}}}{G^{\mathrm{N}}_{\mathrm{M}}} = -\frac{p'_t}{p'_l} \cdot \frac{(E_e + E_{e'}) \tan(\theta_e/2)}{2m_{\mathrm{N}}} \,. \qquad (9)
$$

An important question is to what extent that this equation is valid. Then, one has to test our understanding of the polarization observables in the $^2\mathrm{H}(\vec{e}, e'\vec{p})n$ reaction.

In the following, we will take the consistent, state-of-art calculations by Arenhövel *et al.* [19, 22] as a guideline to discuss theoretical predictions for our proposed measurements. The calculations are in a non-relativistic approach, and the two-nucleon bound

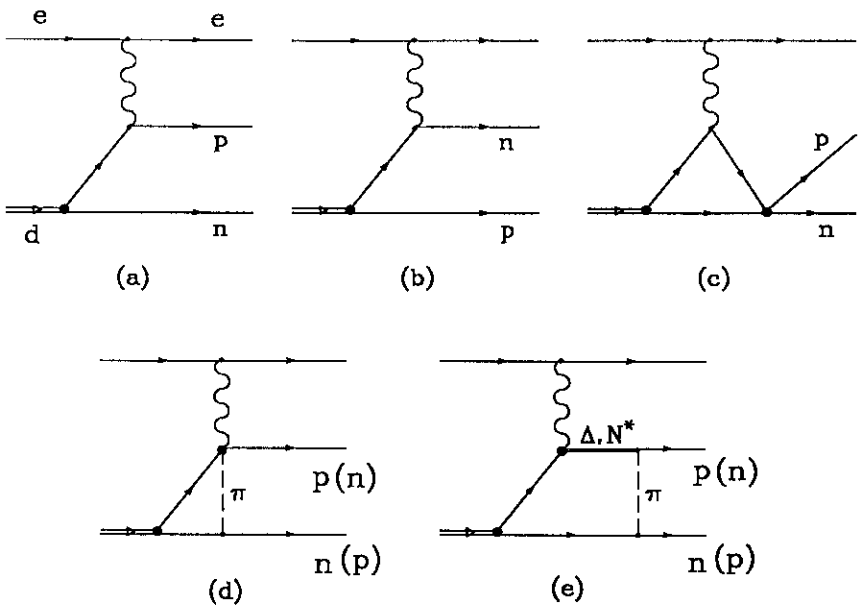

Figure 2: Schematic diagrams contributing to the ^{2}H$(e,e'p)n$ cross-section. (a) PWIA e-p scattering, (b) PWIA e-n scattering, (c) final-state interactions, (d) pion exchange one-body, pair, contact and meson currents, and (e) isobar excitations.

and scattering states are computed by solving the Schödinger equation using a potential description for the NN interaction. Their model includes nucleon resonance configurations and relativistic corrections. The relativistic effects are included by a non-relativistic expansion in orders of (p/M). Moreover, they took into account the contributions from π, ρ and ω exchange currents. Fig. 2 shows the most important lowest-order diagrams included in the calculations. The Born approximation (BA) neglects the final-state interaction between the outgoing proton-neutron pair, and MEC and IC effects, but still retains the electromagnetic interaction with the neutron (diagram b).

Fig. 3, 4, 5 and 6 show the results of calculations from Arenhövel *et al.* [22] with the Paris potential [34]. The calculations were performed at the proposed kinematics, i.e. in Δ region, with $Q^2 = 0.26$ (GeV/c)^2 ($q = 645$ MeV/c and $\omega = 400$ MeV). The electron beam energy is assumed to be 1.645 GeV and scattered electrons detected at 20.4°. Different curves indicate the various ingredients included in the calculations. In the figures, the statistical uncertainties which are expected from the proposed measurements are also displayed.

The proposed kinematics has been optimized with the physics goal in a limited beam time. Note that, the proposed measurements are intended as a starting point for such a study so that only one Q^2 point is considered in the present. Possible study on the Q^2 dependence will be evaluated shortly after this initial measurement.

Fig. 3 shows the components of recoil proton polarization and the cross section. Fig. 4 displays the ratio of the two components of polarization p'_t and p'_l in the form of the right-hand side of Eq. 9. With measured cross sections and polarization components, one can form the asymmetry $A_{LT'}$ and can extract the individual structure functions, as shown

in Fig. 5 and 6.

We briefly discuss some interesting observations.

- As shown in Fig. 3, at θ_{pq}^{cm}=0°, both p_l' and p_n^0 exhibit contributions from the FSI, especially p_n^0. While the MEC and IC contribute about 1/3 of the cross section at θ_{pq}^{cm}=0°, they do not affect much of the polarization components. However, when the kinematics is moved away from parallel, the MEC and IC start to affect the polarization components. At large θ_{pq}^{cm} angles, the contributions from the MEC and IC dominate not only the cross section but also the polarization components.

- This can be further seen in Fig. 4. For a Fermi-gas model with a plane wave impulse approximation, one would expect the weighted p_t'/p_l' ratio to be 1. However, the models from Arenhövel *et al.* predict a large deviation from 1 and the full model predicts zero for $\theta_{pq}^{cm} \leq -40°$. The effects of including FSI, MEC and IC are obvious. It is also interesting to note that at θ_{pq}^{cm}=0°, where the ratio is insensitive to the MEC and IC, the PWBA+RC model gives a close to 1 prediction for the bound proton with a initial momentum of 260 MeV/c, while the N+RC model predicts an approximately 30% lower value.

- In A_{LT} as shown in Fig. 5, relativistic effects dominate. However, one sees the competing effects from FSI. For small θ_{pq}^{cm} angles, the two contributions cancel each other almost entirely, so that the PWBA model gives roughly the same results as the full calculation. At large θ_{pq}^{cm} angles, the effects of FSI becomes large. However, relativistic effects are still discernible.

- Fig. 6 shows the rich deuteron physics with measurements of separated structure functions. We can see some simplicities from the results of the calculations. At θ_{pq}^{cm}= 0°, f_{LT}^n is dominated by the FSI, and $f_{LT}^{\prime t}$ and $f_T^{\prime l}$ originate mostly from the electromagnetic properties of the nucleon. At $\theta_{pq}^{cm} \neq 0°$, $f_T^{\prime t}$ is entirely due to the IC. Furthermore, one can see the similarities (up to a minus sign) between f_{LT} and $f_{LT}^{\prime l}$ and between $f_L + \frac{\rho_T}{\rho_L} f_T + \frac{\rho_{TT}}{\rho_L} f_{TT}$ (which is dominated by f_T in this case) and $f_T^{\prime l}$. Therefore, by measuring all of them, one can have a stringent test of the components of the theory.

It is clear that the polarizations and extracted structure functions are very sensitive to the inclusion of final-state interactions, meson-exchange currents, isobar contributions and relativistic effects. Moreover, different quantities display quite different sensitivities to various ingredients included in the calculations. In some of them, the various effects cancel each other. Therefore, it is necessary not only to separate them but also to measure as many as possible.

The statistical uncertainties in the figures and possible systematic uncertainties, which will be discussed in Sec. 5, show that we will be able to obtain high quality data. We believe that such a set of high quality data, which is presently not available, will be extremely important to constrain the deuteron models.

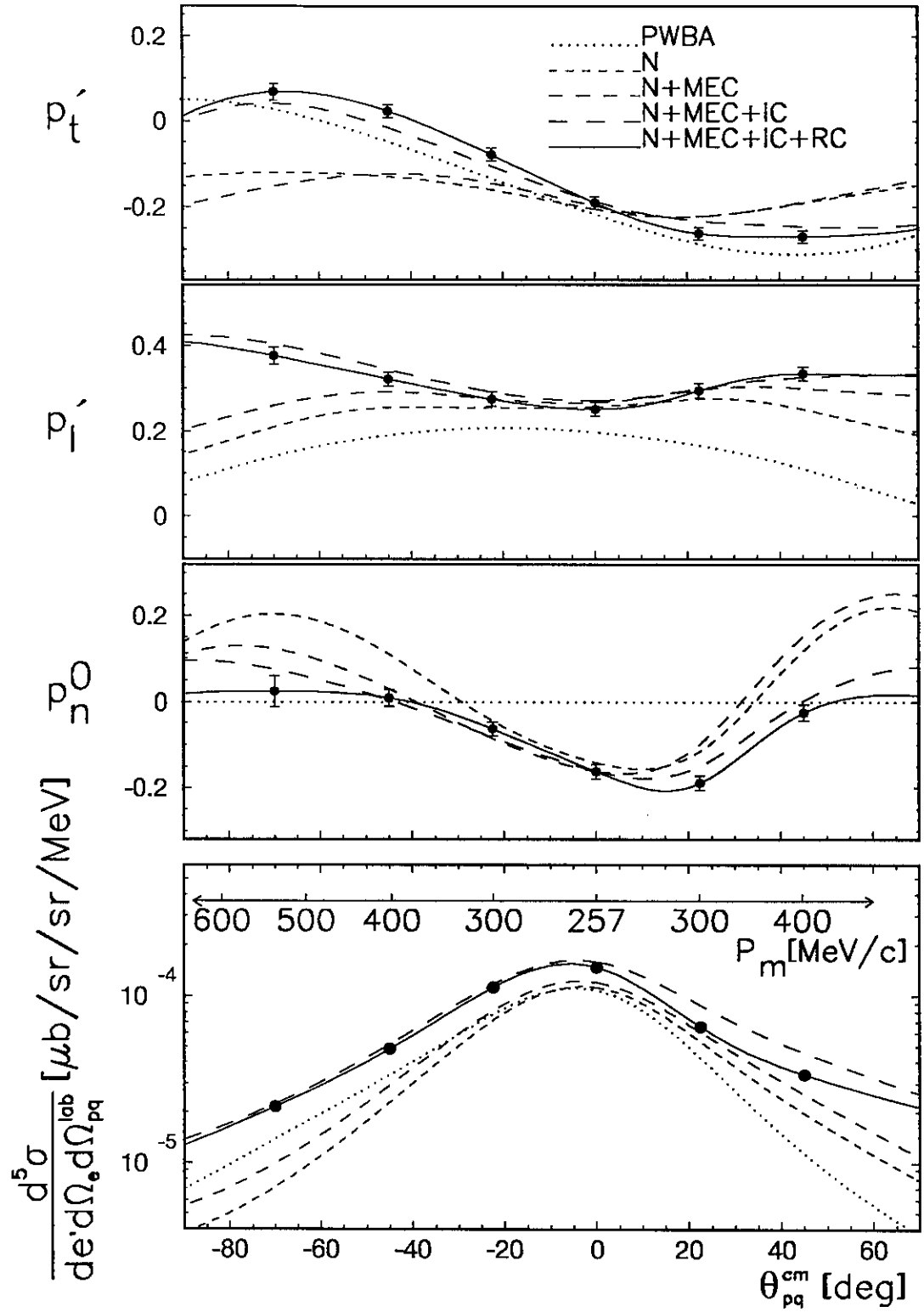

Figure 3: Projected statistical uncertainties in the polarizations p_t', p_l', p_n^0 and the cross-section as functions of θ_{pq}^{cm} at Δ kinematics. The curves are calculations by Arenhövel *et al.* [19] with different ingredients included ("N" stands for FSI).

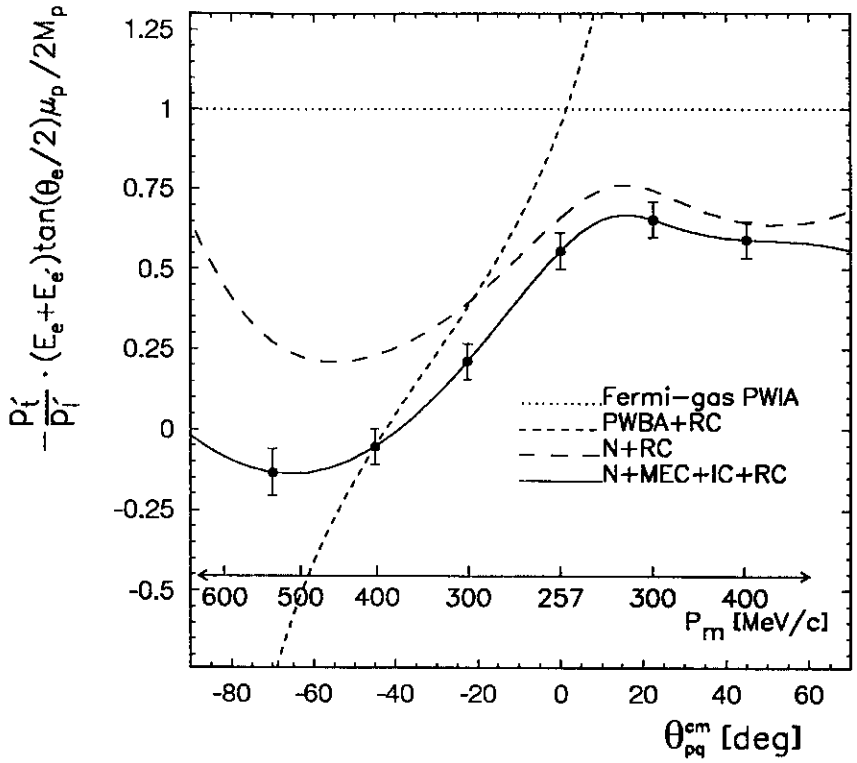

Figure 4: Projected statistical uncertainties in the ratio of $-\frac{p_t'}{p_l'} \cdot \frac{\mu_p(E_e + E_{e'})\tan(\theta_e/2)}{2m_p}$ as functions of θ_{pq}^{cm} at Δ kinematics. The curves are calculations by Arenhövel *et al.* [19] with different ingredients included.

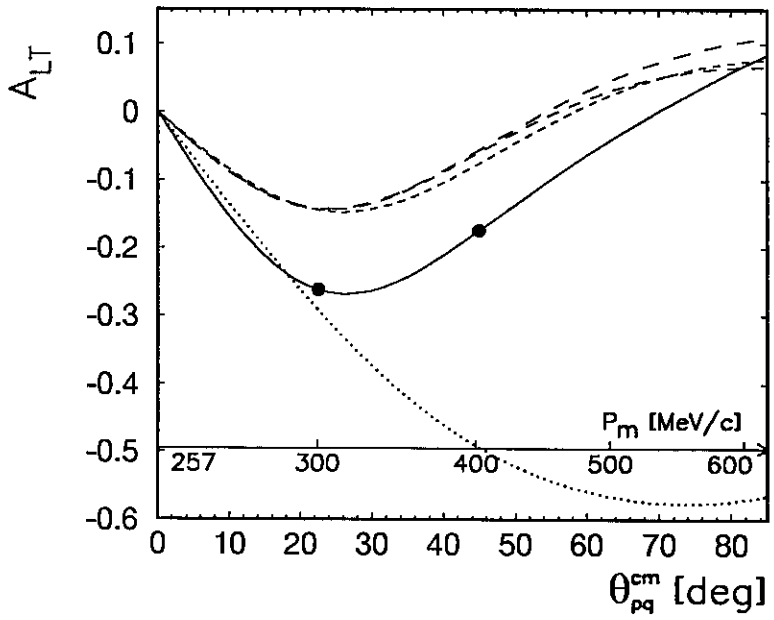

Figure 5: Projected statistical uncertainties in A_{LT} as functions of θ_{pq}^{cm} at Δ kinematics. Notation of curves are as same as in Fig. 3.

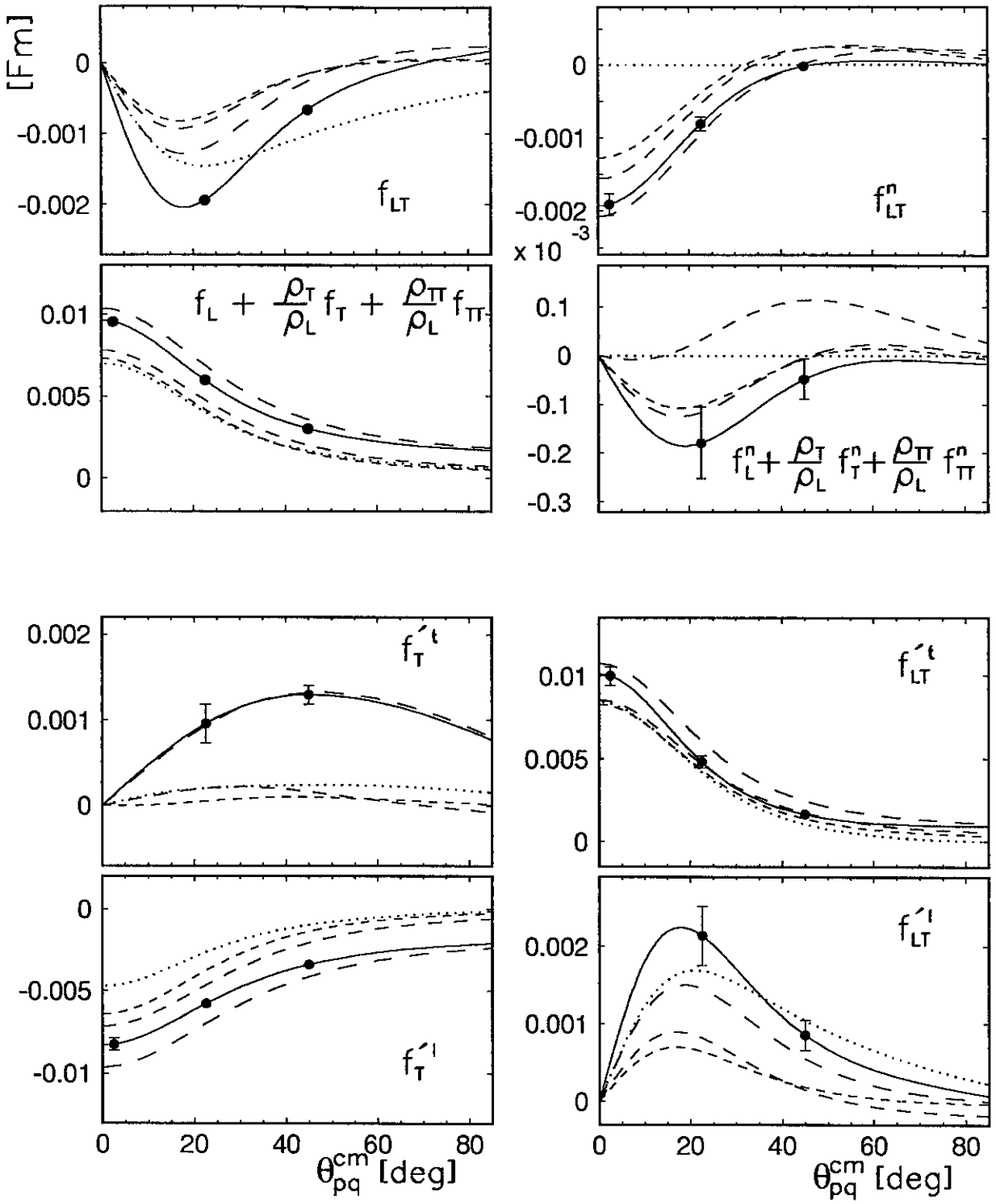

Figure 6: Projected statistical uncertainties in the structure functions $f_{\rm LT}$, $f^n_{\rm LT}$, $f_{\rm L}+\frac{\rho_{\rm T}}{\rho_{\rm L}}f_{\rm T}+\frac{\rho_{\rm TT}}{\rho_{\rm L}}f_{\rm TT}$, $f^n_{\rm L}+\frac{\rho_{\rm T}}{\rho_{\rm L}}f^n_{\rm T}+\frac{\rho_{\rm TT}}{\rho_{\rm L}}f^n_{\rm TT}$, $f'^t_{\rm T}$, $f'^t_{\rm LT}$, $f'^l_{\rm T}$, and $f'^l_{\rm LT}$ as functions of $\theta^{\rm cm}_{\rm pq}$ at Δ kinematics. Notation of curves are as same as in Fig. 3.

4 Experimental plan

In this section, we will discuss details of the proposed measurements. We plan to use the two HRS spectrometers, the focal–plane polarimeter and the existing cryogenic liquid deuterium target in Hall A. The measurements will utilize the polarized electron beam.

4.1 Detector configurations

Fig. 7 shows the layout of the detector configurations for the measurements of the $^2\mathrm{H}(\vec{e}, e'\vec{p})n$ reaction in the Δ-kinematics. All the directions are in the scattering (horizontal) plane.

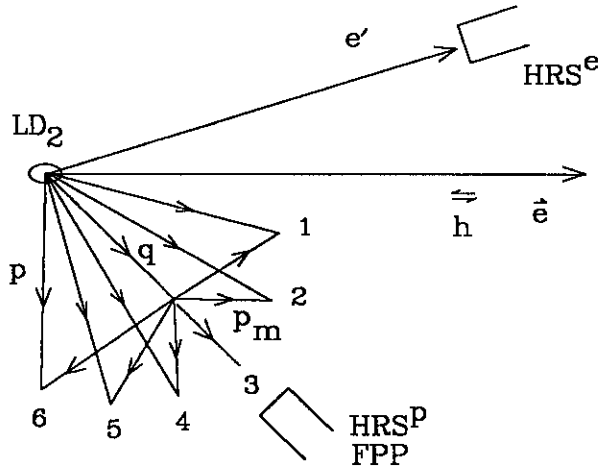

Figure 7: Schematic outline of the experimental configurations for the parallel (3) and non-parallel kinematics (1, 2, 4, 5 and 6) at the same electron Δ-kinematics: HRS^e is used to detect scattered electrons from the cryogenic liquid deuterium target (LD_2) in coincidence with the knock-out protons detected and polarization-analyzed in HRS^p and FPP.

We have tried to optimize the kinematics with consideration in achieving the physics goal with a limited beam time. We choose the kinematics $(\vec{q}, \omega) \simeq$ (645 MeV/c, 400 MeV). In this region the various effects as discussed previously are expected to be large and the knock-out protons have kinetic energies in a range of 250-360 MeV, which results in a high figure of merit for the focal-plane polarimeter. Fortunately, data exist from Bates previous measurements for quasi-elastic and "dip" kinematics at the same $\mid \vec{q} \mid$ [38, 39]. Therefore, our proposed measurements in the "Δ"-kinematics can be compared with the existing data.

This experiment can only be performed in Hall A at TJNAF because of the counting rates and optimization of the sensitivity to the interesting observables. We plan to use a standard beam energy of 1.645 GeV and to detect the scattering electrons at 20.4°. This choice of parameters has the advantage of a high counting rates at a low momentum transfer compared to other electron facilities. In addition, the spin precession in a 45° bending

spectrometer favors the measurements of p'_l for protons with kinetic energies ranging from 250 to 360 MeV. This advantage, as will be shown later, gives an order of magnitude increase in the figure of merit for the measurements of p'_l polarization compared to Bates and Mainz.

We intend to use the cryogenic liquid deuterium target, both high-resolution spectrometers and the focal-plane polarimeter for the measurements. In the detector configurations shown in Fig. 7, HRS$^{\rm e}$ is set at the same scattering angle and the same central momentum to detect the scattered electrons in coincidence with the knock-out protons in HRS$^{\rm p}$. The measurements will be performed in six different hadron kinematics: $\theta_{\rm pq}^{\rm cm} \simeq$ +45°, +22.5°, 0°, −22.5°, −45° and −70°, which correspond to $p_m \simeq$ 403, 301, 257, 301, 403 and 537 MeV/c respectively, while keeping the same electron kinematics.

Kin	E_o MeV	θ_e (°)	ω MeV	q MeV/c	θ_q (°)	q_μ^2 fm^{-2}	E_{np} MeV	θ_p (°)	p_p MeV/c	$\theta_{\rm pq}^{\rm cm}$ (°)	p_m MeV/c
1	1645	20.4	400	645	−42.2	6.6	304	−14.0	831	45.0	403
2	1645	20.4	400	645	−42.2	6.6	304	−28.3	884	22.5	301
3	1645	20.4	400	645	−42.2	6.6	304	−42.2	902	0.0	257
4	1645	20.4	400	645	−42.2	6.6	304	−56.2	884	−22.5	301
5	1645	20.4	400	645	−42.2	6.6	304	−70.5	831	−45.0	403
6	1645	20.4	400	645	−42.2	6.6	304	−87.3	737	−70.0	537

Table 1: Kinematical quantities for the proposed measurements.

Tab. 1 shows the detailed kinematic settings for the measurements. $\theta_{\rm e,p}$ show HRS$^{\rm e,p}$ angles in the laboratory frame, and $E_0 - \omega$ and p_p are the central momenta of the scattered electrons and the knock-out protons. Negative $\theta_{\rm q}$ and $\theta_{\rm p}$ mean they are opposite to the scattered electron side. Positive $\theta_{\rm pq}$ means $\phi_{\rm pq}^{\rm cm} = 0°$ while negative $\theta_{\rm pq}^{\rm cm}$ means $\phi_{\rm pq}^{\rm cm} = 180°$. The kinematics are in the Δ region ($E_{\rm np} = 304$ MeV and $q_\mu^2 = 6.6$ fm^{-2}) away from the quasi-elastic ridge. The different $\theta_{\rm pq}^{\rm cm}$ settings are obtained by changing the angle and central momentum of HRS$^{\rm p}$ during the measurements.

	$\Delta p/p$ %	$\delta p/p$ $\times 10^{-4}$	Δy cm	δy mm	$\Delta\theta$ mrad	$\Delta\phi$ mrad	$\delta\theta$ mrad	$\delta\phi$ mrad	$\Delta\Omega$ msr
HRS$^{\rm e}$	±4.5	2.5	±5	1.5	±60	±28	2.0	0.6	6.7
HRS$^{\rm p}$	±4.5	2.5	±5	1.5	±60	±28	2.0	0.6	6.7

Table 2: Some properties of the high resolution spectrometers at Hall A.

Tab. 2 lists some of the measured properties of both electron and hadron high-resolution spectrometers. We do not need any special hardware change and/or development for either spectrometer in running this experiment. We anticipate a few experiments to be finished in the first-running period of Hall A so that we will have a good understanding of the spectrometers and the focal-plane polarimeter. These have been demonstrated by the two Oxygen experiments (E89-003 and E89-033) completed recently. In the next section, we briefly discuss the requirements on the polarized beam and the cryogenic liq-

uid deuterium target, and later we will show the formalism and estimates in using the focal-plane polarimeter.

4.2 Polarized beam

We assume a CW polarized electron beam with an averaged current of at least 50 μA and a polarization of approximately 40% for the proposed measurements.

The polarized electron CW beam will be used in several experiments in the first-running period at Hall A. At present, the accelerator is able to deliver currents in excess of 50 μA with a polarization of approximately 40% to Hall A when the other two halls are running. Experience with the operation of polarized beam will increase with time. Stabilities of the current and polarization over helicity flips can be better than 10^{-5}, which exceeds the requirements of this proposed experiment by several orders of magnitude. We assume that operation of the beam will be stable and, therefore, in our count rate estimates we make no provision for down time due to beam problems.

The development of high polarization source based on strained GaAs crystals will be highly beneficial to our proposed measurements. Since the experimentally measured helicity-dependent polarizations $p_{X,Y}$ are proportional to the beam polarization p_e (see Sec. 4.4), a factor of 2 increase in the beam polarization would improve the measurements in the figure of merit by a factor of 4.

The beam polarization will be monitored with the Hall-A Möller polarimeter (and/or the laser-back-scattering polarimeter). One Möller measurement takes typically less than 10 min. Currently, the measurement error of the polarization is $\lesssim 4.5\%$. In our beam-time request we include beam time needed for the periodical Möller measurements. Furthermore, the highest statistical precision used for our count rate estimates does not exceed about 5% in the quantities of $\delta p_{X,Y}/p_{X,Y}$ as will be discussed in Sec. 4.5, so that the uncertainty in the beam polarization is not the limiting factor in this measurement.

4.3 LD_2 cryo-target

We plan to use the present cryogenic liquid deuterium target in Hall A. The target has been successfully commissioned during the recently finished experiment measuring the deuteron elastic structure functions (E91-026). The detailed description of the target can be found in the Hall-A web pages. In the following, we briefly listed the specifications of the target relevant to our luminosity discussion:

- **Target length**: 4 and 15 cm for 2 different cells
- **Target density**: 166 mg/cm^3
- **Operating condition**: 22 K (LD_2) / 19 K (LH2), 2 Atm

- **Beam current**: $\geq$ 70 μA
- **Cooling power**: $\geq$ 500 Watts

With a 50 μA beam current and a 15 cm target length (assuming 8cm visible to spectrometers), the luminosity is about 1.2×10^{38} ^{2}H$\cdot$cm$^{-2}\cdot$s^{-1}. This value will be sufficient for our measurements (see Sec. 4.5). The singles rates for various reaction channels are expected at a reasonable level as seen from Tab. 4 in Sec. 4.5. Background events from the target entrance and exit windows can be measured and subtracted with an equivalent "empty" target of the same geometry filled with either liquid or gaseous hydrogen. In addition, one can apply a vertex cut to the data since both HRS^{e,p} have a good vertex resolution ($\delta y \sim$ 1.5 mm). Furthermore, we can apply a missing mass cut around the deuteron binding energy (the missing mass resolution has been shown to be about 1-2 MeV from E89-003). Therefore, we do not expect a significant background contribution to the $^2\mathrm{H}(\vec{e},e'\vec{p})n$ counting rates.

4.4 Focal-plane polarimeter

A full description of this polarimeter can be found elsewhere. In the following, we briefly discuss the basics relevant to the estimate of statistical uncertainties for our proposed experiment.

The cross-section for the secondary scattering of the outgoing polarized proton from an analyzer can be written as:

$$\sigma = \sigma_0(\theta_2)[1 + A_y(\theta_2)(p_X \sin\phi_2 + p_Y \cos\phi_2)]\,, \tag{10}$$

where θ_2 and ϕ_2 are the polar azimuthal angles of the secondary scattering, A_y is the analyzing power, σ_0 is the unpolarized cross section and $p_{X,Y}$ are the polarization components. The polarimeter coordinates system is defined as X-axis along the momentum dispersion direction, Z axis along the proton momentum direction and Y axis normal to the bend plane based on the right-hand rule. By measuring the ϕ_2 distribution in the polarimeter one can disentangle the polarization components p_X and p_Y.

To calculate the statistical precision, only those protons scattered in the analyzer and in coincidence with detected electrons are considered. The Coulomb scattering in the analyzer dominates for small polar scattering angles and it provides no polarization information. Only the nuclear scattering at large proton angles ($\gtrsim 4°$), gives A_y which is substantially different from zero.

After some algebra following Eq. 10, one can obtain the statistical uncertainty (assuming Gaussian distributions and no instrumental asymmetries) in either polarization component:

$$\delta p_{X,Y} = \frac{\pi}{2\langle A_y\rangle}\sqrt{\frac{1}{f\cdot N}}\,. \tag{11}$$

$\langle A_y \rangle$ is the analyzing power averaged over an angular cone for which A_y is substantially different than zero, f is the fraction of events that scatter into this cone and N is the total number of events detected in the spectrometer focal plane in coincidence with electrons detected on the opposite side.

One intends to measure the polarization components, for example, p'_t, p'_l and p^0_n resulting from the primary scattering. However, some of these polarization components will precess when protons pass through the magnetic spectrometer. To a simple dipole approximation, the transverse polarization component does not precess. On the other hand, the normal and longitudinal components precess about the spectrometer magnetic field direction. Thus, in general, the polarimeter is capable of measuring the transverse components as well as a mixture of the longitudinal and normal components. However, because the p'_l polarization is helicity dependent while the normal term p^0_n is helicity independent, both the normal and longitudinal components can be separated by flipping the helicity of the electron beam. Explicitly, we have for the components of polarization after precession by an angle χ through the spectrometer:

$$\begin{aligned} p_X &= p^0_n \cos\chi + h \cdot p_e \cdot p'_l \sin\chi \\ p_Y &= h \cdot p_e \cdot p'_t \\ p_Z &= -p^0_n \sin\chi + h \cdot p_e \cdot p'_l \cos\chi \,. \end{aligned} \tag{12}$$

The precession angle is given by

$$\chi = \frac{g-2}{2}\gamma\,\Omega_B \,, \tag{13}$$

where g is the proton gyromagnetic ratio (=5.586), γ is the Lorenz factor and Ω_B is the total bend angle for the spectrometer. One obtains directly p'_t from p_Y and a clear separation of p'_l and p^0_n from p_X through the use of the electron helicity, *i.e.*:

$$\begin{aligned} p'_t &= \frac{p_Y(h=+1) - p_Y(h=-1)}{2p_e} \\ p'_l &= \frac{p_X(h=+1) - p_X(h=-1)}{2p_e \sin\chi} \\ p^0_n &= \frac{p_X(h=+1) + p_X(h=-1)}{2\cos\chi} \,. \end{aligned} \tag{14}$$

Combining Eq. 11, 12 and 14 one then have statistical uncertainties for all three polarization components:

$$\begin{aligned} \delta p'_t &= \frac{\pi}{2p_e \cdot \langle A_y \rangle}\sqrt{\frac{1}{f \cdot N}} \\ \delta p'_l &= \frac{\pi}{2p_e \cdot \langle A_y \rangle \sin\chi}\sqrt{\frac{1}{f \cdot N}} \\ \delta p^0_n &= \frac{\pi}{2\langle A_y \rangle \cos\chi}\sqrt{\frac{1}{f \cdot N}} \,. \end{aligned} \tag{15}$$

Tab. 3 lists the estimated spin-precession angles, carbon block thicknesses, energy losses, multiple scattering angles, efficiencies and averaged analyzing powers for the proposed proton kinematics. The spin-precession angles are estimated with a simple dipole approximation. By limiting the multiple scattering to be <1.5°, one can determine the carbon block thicknesses for the measurements. By requiring the proton scattering angle to be greater than 4°, one can estimate the efficiency f and the averaged analyzing power $\langle A_y \rangle$ for scattered protons. Such estimates are performed using a computer code [44] based on reasonable extrapolated values from recent measurements. Since the protons kinematics are specially designed with averaged kinetic energies in the region of 300 MeV where the analyzing power is large, one sees that both f and $\langle A_y \rangle$ are large for carbon blocks with practical thicknesses.

kin	P (MeV/c)	E (MeV)	χ (deg)	^{12}C thickness (cm)	E_{loss} (MeV)	Mult. Scatt. (deg)	f (%)	$\langle A_y \rangle$
1&5	831	315	108	14	~70	~1.4	~5.0	~0.46
2&4	884	351	111	16	~80	~1.4	~6.0	~0.43
3	902	363	112	17	~85	~1.4	~6.3	~0.42
6	737	255	103	9	~55	~1.4	~3.1	~0.49

Table 3: Estimates of the efficiencies and averaged analyzing powers of the polarimeter for the proposed proton kinematics.

This is further illustrated in Fig. 8, where the figure of merit (f.o.m) for the recoil proton polarimetry in terms of $f \cdot \langle A_y \rangle^2$, $\langle \sin\chi \rangle^2$ and $\langle \cos\chi \rangle^2$ are shown as a function of the proton kinetic energy. In the middle and bottom panels, the solid (dashed) curves represent the polarimetry with a 45° (90°) bending spectrometer. Note that the OHIPS at Bates is a 90° bending spectrometer while HRS^p in Hall A has a 45° bending angle. The solid circles indicate the region where the measurements were performed at Bates, while the open circles show the region of measurements proposed in this proposal. We conclude that our proposed measurements have a much higher f.o.m. for measuring both p'_t and p'_l as well as their ratios. This is important since they are helicity-dependent and the electron beam polarization is around 40% which is low.

With Eq. 15 and experimental conditions listed in Tab. 3, we can now estimate the statistical uncertainties for a given beam time. In the next, we will show a detailed beam-time request and expected qualities of our proposed measurements.

4.5 Beam-time request

The proposed kinematics and the estimated count rates are shown in Tables 4 and 5. The estimate of counting rates and statistical uncertainties are based on the acceptances of HRS^{e,p} and are calculated using MCEEP [42]. The luminosity assumed is 1.2×10^{38}

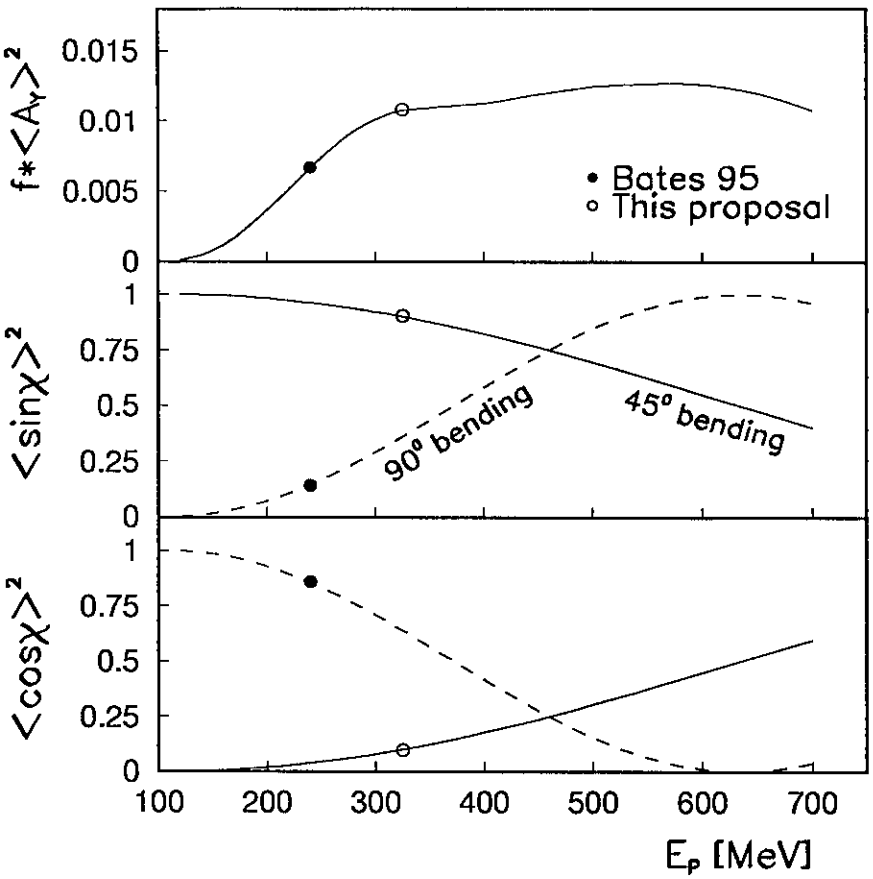

Figure 8: Figure of merit in terms of $f \cdot \langle A_y \rangle^2$, $\langle \sin\chi \rangle^2$ and $\langle \cos\chi \rangle^2$ as a function of the proton kinetic energy. In the middle and bottom panels, the solid (dashed) curves represent the polarimetry with a 45° (90°) bending spectrometer. The solid circles indicate the region where the measurements were performed at Bates, while the open circles show the region of measurements proposed in this proposal.

^{2}H·cm^{-2}·s^{-1} with a 50 μA beam current and a 15 cm cryogenic liquid deuterium target. In addition, the measured spectrometer y-target acceptances are folded. The prescription σ_1^{cc} for the off-shell e-p cross-section and a parameterization of the nucleon momentum density distribution calculated by Van Orden are incorporated into MCEEP. Since the kinematics are in the Δ-region, the IC contributions to the cross-section cannot be neglected. Therefore, overall cross-section values are scaled to match the values of the full model calculations from Arenhövel *et al.* [22]. Thus the rates as well as the beam-time estimates are considered to be very realistic. We intend to run in conjunction with other experiments using the same cryogenic target. Therefore, we do not expect over-head time such as for the target installation.

The estimated singles count rates and accidental coincident rates are also shown in Table 4. The singles count rates (those observed in HRS^e originating from the (e,e') and (e,π^-) reactions and in HRS^p originating from the (e,p) and (e,π^+) reactions) are estimated with the computer codes QFS and EPC of Lightbody and O'Connell [43]. Accidental coincidence rates were calculated assuming a coincidence timing width of 2 ns and a duty factor of 100%. The listed accidental rates are over the whole missing

		Singles				Raw Acc.	Trues/Acc.
Kin	$HRS^{e,p}$ central kinematics	(e,e') (kHz)	(e,π^-) (kHz)	(e,p) (kHz)	(e,π^+) (kHz)	$(e,e'p)$ (Hz)	$(e,e'p)$ w/ cuts
	θ_e= 20.4° e'= 1245 MeV/c	98	16				
1	θ_p= −14.0° p_p= 831 MeV/c			17	11	4	$\gtrsim$ 500
2	θ_p= −28.3° p_p= 884 MeV/c			4.3	∼0	1	$\gtrsim$ 500
3	θ_p= −42.2° p_p= 902 MeV/c			4.3	∼0	1	$\gtrsim$ 500
4	θ_p= −56.2° p_p= 884 MeV/c			4.3	∼0	1	$\gtrsim$ 500
5	θ_p= −70.5° p_p= 831 MeV/c			4.3	∼0	1	$\gtrsim$ 500
6	θ_p= −83.7° p_p= 737 MeV/c			4.3	∼0	1	$\gtrsim$ 500

Table 4: Estimates of singles and raw accidentals rates and the trues-to-accidental ratios for the proposed kinematics. The electron beam is assumed with an energy of 1.645 GeV and a current of 50 μA, in use with a cryogenic liquid deuterium target of 15 cm.

θ_{pq}^{cm} (deg)	N (Hz)	N·f (Hz)	N·f_{total} required	$\delta p_{X,Y}$	$\delta p_t'$	$\delta p_l'$	δp_n^0	beam time (hrs)
+45	14.7	0.74	324000	0.006	0.015	0.016	0.019	123
+22.5	32.9	1.97	371000	0.006	0.015	0.016	0.017	54
0	68.5	4.32	388000	0.006	0.015	0.016	0.017	26
−22.5	48.6	2.90	371000	0.006	0.015	0.016	0.017	37
−45	22.2	1.11	324000	0.006	0.015	0.016	0.019	83
−70	10.3	0.32	161000	0.008	0.020	0.020	0.036	142
							Total:	465
							Starting preparation:	8
							Möller polarization measurements:	15
							Angle changes overhead:	20
							Hydrogen calibration measurements:	20
							Grand Total:	528

Table 5: Estimates of trues count rates and statistical errors at a given beam time, and consequently summary of the beam time request.

energy range within the momentum acceptances of the spectrometers. Since the electrons detected in HRS^e and the protons detected in HRS^p can be well-selected with the particle identifications, accidentals rates caused by (e,π^-) and (e,π^+) reactions are not included and they are expected to be small as seen from Tab. 4. When the reaction $^2H(e,e'p)n$ is selected, a cut on the missing-mass peak (at the deuteron binding energy) is applied.

The accidentals within the cut will be about a factor of ~20 less than the listed numbers since the accidental events will be distributed over the entire missing-mass acceptance. In addition, the accidental events tend to have random vertex distributions for electrons and protons. Therefore, one can apply a vertex correlation cut to further suppress the accidentals since both HRS^{e,p} have good vertex resolutions ($\delta y \sim 1.5$ mm). Consequently, as shown in Table 4, the accidental coincidence rates are insignificant compared to the true coincident rates listed in Table 5, so that very high trues-to-accidentals ratios can be obtained. Furthermore, the singles rates are extremely low so that they will not add much to the detector dead-time.

The beam-time estimates for each kinematic point are based on the sensitivities of measurements to the physics goals, and the final expected statistical uncertainties are kept >0.015 for p'_l, p'_t and p^0_n. Tab. 5 lists the time requested for each kinematics and summarizes the detailed break-down of beam time. This includes time for starting preparation, measurements of the beam polarization (Möller), ^{1}H(e,e') and ^{1}H(e,p) single-arm relative efficiency calibrations, ^{1}H$(\vec{e},e'\vec{p})$ calibration measurements and over-head in angle changes for HRS^p, but does not include down time.

The final statistical errors are shown in Tab. 5. Since the proton particle identification is done in front of the carbon-analyzer at the HRS^p focal plane, one can obtain simultaneous data on the differential cross-section for the ^{2}H$(\vec{e},e'\vec{p})n$ reaction at the same kinematics without requiring any additional beam time. With measured cross sections and polarizations, one can consequently extract the structure functions. The quality of our proposed measurements of polarizations and the corresponding extracted structure functions has been shown in Fig. 3, 4, 5 and 6. We will discuss possible systematic uncertainties next.

5 Systematic Uncertainties

This proposed experiment involves measuring a variety of physics quantities, with which the associated possible systematic uncertainties are quite different. For example, in the measuring the polarization components and $A_{LT'}$, asymmetries rather than absolute cross sections play the important role. p'_l and p'_t depend on the incident electron helicity, so that, most of the instrumental systematic uncertainties cancel. In extracting structure functions, one needs to determine the absolute cross sections. Note that, some of the discussion below have been presented in detail in the E89-003 experiment handbook [45].

The Hall spectrometer pair, along with the high quality beam at JLab, will provide superb definition of the event-by-event kinematics. A momentum resolution of 2-4$\times10^{-4}$ in both the incident and scattered electron energies and an angular resolution of 0.5 mrad will results in a Q^2 resolution of 1-3$\times10^{-3}$ (GeV/c)^2 and a missing mass resolution of ~1 MeV. With additional contributions from the alignment of spectrometers (~0.5 mrad), an absolute resolution of $\lesssim$3 mrad in θ^{lab}_{pq} $(= \theta_q - \theta_p)$ can be straightforward. This will give us a resolution of $\lesssim$5 mrad for the θ^{cm}_{pq} angles.

For the cross section measurements, we take the approach that a 3% absolute determination is possible. This has been an accepted assumption for many proposed measurements in Hall A. As shown in Fig. 3 bottom-panel, a 3% systematic uncertainty will not seriously affect the quality of our measurements.

Assuming that only the Möller polarimeter is available for measuring the beam polarization, one can have a possible uncertainties of $\lesssim 4.5\%$ in the electron beam polarization. (The beam polarization can also be determined in Hall A via a couple of other methods, for example, ^{1}H$(\vec{e}, e'\vec{p})$ measurements and the Laser back-scattering. So, an accuracy better than 4.5% can be expected. Nevertheless, we assume a conservative value of 4.5% in our estimate.) In addition, there is an uncertainty of $\lesssim 1.5\%$ in the p-^{12}C analyzing power, A_y. Therefore, we anticipate that a systematic uncertainty of 5.0% is possible for both $\delta p'_t/p'_t$ and $\delta p'_l/p'_l$. This uncertainty will cancel in the measurements of the ratio of p'_t/p'_l, as shown in Fig. 4. In the first order, as shown in Eq. 14 and/or 15, p'_t is independent of the spin-precession angle χ while p'_l is proportional to $1/\sin\chi$. Hence, there is an additional systematic uncertainty in p'_l associated with the determination of the angle χ. However, this is suppressed in our kinematics since $\sin\chi$ are close to 1.

The systematic uncertainty in $p^0_{\rm n}$ has been studied substantially during the FPP commissioning experiment E89-033, where the unpolarized e-p elastic scattering was used. A value of $\lesssim 0.002$ in the raw asymmetry has been achieved [46]. Given an amplification factor caused by $1/\cos\chi$ ($\sim$3-4) in our kinematics, we assume that a systematic uncertainty of 0.010 can be possible in $\delta p^0_{\rm n}$ (absolute).

In order to extract the structure functions, one has to combine two measurements on both sides of the momentum transfer direction. Then, the systematic uncertainties comes from the determination of angles (mainly θ_q and θ_p), the determination of the cross sections, and the determination of polarization components. To illustrate the size of possible systematic uncertainties in the structure functions, we take the combination of Kin #2 and #4 as an example as shown in Tab. 6. In this estimate, we use the full calculations (N+MEC+IC+RC) by Arenhövel *et al.* [19] as a guideline. We assume that possible sources for systematic uncertainties are $\delta\theta^{\rm cm}_{\rm pq} \leq 5.0$ mrad, $\delta\sigma/\sigma \leq 3.0\%$, $\delta p'_t/p'_t \leq 5.0\%$, $\delta p'_l/p'_l \leq 5.0\%$ and $\delta p^0_n \leq 0.010$. The total systematic uncertainties are a summation in quadrature. For comparison, the statistical uncertainties from the proposed measurements are also listed in the last column. In order to avoid double counting of uncertainties, we only calculate the direct effects from $\theta^{\rm cm}_{\rm pq}$. (Obviously, the uncertainties in $\theta^{\rm cm}_{\rm pq}$ will cause errors in the cross sections, which eventually cause uncertainties in structure functions. However, these have been counted as the contributions from the cross sections in our estimate.) We neglect the contributions from ϕ_e and ϕ_p angles, which are mostly suppressed due to $\cos\phi^{\rm cm}_{\rm pq}$ factors for in-plane kinematics.

As seen from Tab. 6, most of systematic uncertainties are smaller than the expected statistical errors. Note that the high statistical precision in $f_{\rm LT}$ and $f_{\rm L} + \frac{\rho_{\rm T}}{\rho_{\rm L}} f_{\rm T} + \frac{\rho_{\rm TT}}{\rho_{\rm L}} f_{\rm TT}$ originates from the fact that no recoil polarization measurements are required.

The above discussion on possible systematic uncertainties is based on present understanding of the equipments and hence takes a conservative approach. We anticipate a

better understanding of systematic uncertainties as time progresses.

	$\delta\theta_{pq}^{cm}$ 5.0 mr	$\delta\sigma/\sigma$ 3.0%	$\delta p_t'/p_t'$ 5.0%	$\delta p_l'/p_l'$ 5.0%	δp_n^0 0.010	tot. syst. uncert.	stat. uncert.
$\delta f_{LT}/f_{LT}$ (%)	0.6	8.4	-	-	-	8.4	0.1
$\delta(f_L+...)/(f_L+...)$ (%)	1.2	2.2	-	-	-	2.5	0.05
$\delta f_{LT}^n/f_{LT}^n$ (%)	2.5	2.2	-	-	6.7	7.5	11.4
$\delta(f_L^n+...)/(f_L^n+...)$ (%)	0.6	8.0	-	-	24.4	25.9	41.4
$\delta f_T'^l/f_T'^l$ (%)	0.9	2.2	-	3.7	-	4.4	4.1
$\delta f_{LT}'^l/f_{LT}'^l$ (%)	0.6	9.5	-	15.8	-	18.4	18.1
$\delta f_T'^t/f_T'^t$ (%)	1.6	6.9	11.6	-	-	15.6	23.3
$\delta f_{LT}'^t/f_{LT}'^t$ (%)	1.8	2.2	3.8	-	-	5.0	7.5

Table 6: Estimates of possible systematic uncertainties for the structure functions extracted from the combination of Kin #2 and #4 (as an example). The estimate are based on the full calculations by Arenhövel *et al.* [19]. We assume that possible sources for systematic uncertainties are $\delta\theta_{pq}^{cm} \leq 5.0$ mrad, $\delta\sigma/\sigma \leq 3.0\%$, $\delta p_t'/p_t' \leq 5.0\%$, $\delta p_l'/p_l' \leq 5.0\%$ and $\delta p_n^0 \leq 0.010$. The total systematic uncertainty is a sum in quadrature. In comparison, the statistical uncertainties from the proposed measurements are also listed in the last column.

6 Summary

We propose to perform measurements of the polarization components in the reaction $^2\mathrm{H}(\vec{e},e'\vec{p})n$ in the Δ kinematics region. The experiment exploits the high energy, high intensity and high duty-factor polarized electron beam at the JLab in combination with the precise proton polarimeter in Hall A. The combined knowledge of electron and proton spin enables a precise structure-function separation and consequently a stringent test to theory.

We have an intention to submit this proposal as a Hall A collaboration proposal. However, we did not finish it early for a collaboration review before submission. At this time, we intend to submit it as a non-collaboration proposal. In the mean time, we are still seeking for a review in the collaboration. The list of our contributors to this proposal has already indicated that such an endorsement from the collaboration will be soon available. And we are confident that this will be the case before the defense presentation.

We have preliminarily identified two MIT graduate students (among Z. Cai, M. Ruachev and B. Zhang) who can be Ph.D. candidates doing dissertation on this proposed experiment. They can soon come to and reside at JLab after their exams to participate in Hall A experiments.

Supporting graduate study has been a commitment in Hall A collaboration and within many collaboration institutions. Presently, there are a number of graduate students from

many Hall A collaboration institutions on-site to work on many experiments in Hall A. We also have two graduate students (J. Gao and N. Liyanage) on site for extensive time for Hall A commissioning experiments, especially E89-003. It has been our commitment from MIT to keep supporting graduate students on-site.

In a summary, this proposed experiment requires no additional hardware development and resources, only beam time. 528 hours of beam are requested.

References

[1] T.W. Donnelly and A.S. Raskin, Ann. Phys. **169**, 247 (1986).

[2] J.L. Forest *et al.*, Phys. Rev. C **54**, 646 (1996).

[3] H. Arenhövel, W. Leidemann and E.L. Tomusiak, Z. Phys. A **331**, 123 (1988); **334**, 363(E) (1989).

[4] J.D. Bjorken, Phys. Rev. **148**, 1467 (1966); J. Ellis and R.L. Jaffe, Phys. Rev. D **9**, 1444 (1974); **10**, 1669 (1974).

[5] Z.-L. Zhou *et al.*, Nucl. Inst. Meth. A **378**, 40 (1996).

[6] D.G. Crabb and D. Day, in Proc. of the 7^{th} workshop on polarized target materials and techniques, Bad Honnef, Germany, 1994 [Nucl. Inst. Meth. A **356**, 9 (1995)].

[7] S. Kox *et al.*, Nucl. Inst. Meth. A **346**, 527 (1994).

[8] R.W. Lourie *et al.*, IUCF Scientific and Technical Report, 135 (1992 - 1993).

[9] T. Eden *et al.*, Phys. Rev. C **50**, R1749 (1994).

[10] F. Klein *et al.*, Nucl. Phys. A **623**, 323c (1997).

[11] TJNAF proposal E-93-038, "The Electric and Magnetic Form Factors of the Neutron for the ^{2}H$(\vec{e}, e'\vec{n})p$ Reaction", R. Madey *et al.*, TJNAF PAC6 Report, 1993.

[12] TJNAF proposal E-93-026, "The Charge Form Factor of the Neutron", D. Day *et al.*, TJNAF PAC6 Report, 1993.

[13] W. Jaus, Nucl. Phys. A **314**, 287 (1979).

[14] W. Fabian and H. Arenhövel, Nucl. Phys. A **314**, 253 (1979); H. Arenhövel, *ibid.*, **384**, 287 (1982);

[15] M. Bernheim *et al.*, Nucl. Phys. A **365**, 349 (1981); S. Turck-Chieze *et al.*, Phys. Lett. B **142**, 145 (1984).

[16] K.I. Blomqvist *et al.*, private communication.

[17] Z.-L. Zhou *et al.*, submitted for publication (1997); M. Ferro-Luzzi *et al.*, in Proc. of the 15^{th} Int. Conf. on Few-Body Prob. in Phys., Groningen, 1997 (to be published in Nucl. Phys. A).

[18] A. Picklesimer and J.W. Van Orden, Phys. Rev. C **35**, 226 (1987).

[19] H. Arenhövel, W. Leidemann and E.L. Tomusiak, Phys. Rev. C **52**, 1232 (1995); **46**, 455 (1992).

[20] J.A. Tjon, Few-Body Systems Suppl. **5**, 17 (1992); E. Hummel and J.A. Tjon, Phys. Rev. C **42**, 423 (1990); **49**, 21 (1994).

[21] B. Mosconi and P. Ricci, Nucl. Phys. A **517**, 483 (1990); B. Mosconi, J. Pauschenwein and P. Ricci, Phys. Rev. C **48**, 332 (1993).

[22] G. Beck and H. Arenhövel, Few-Body Systems **13**, 165 (1992); Th. Wilbois, G. Beck and H. Arenhövel, *ibid.* **15**, 39 (1993); F. Ritz, H. Göller, Th. Wilbois and H. Arenhövel, Phys. Rev. C **55**, 2214 (1997); Th. Wilbois, P. Wilhelm and H. Arenhövel, preprint MKPH-T-97-19 (LANL: nucl-th/9708005).

[23] S. Gilad, W. Bertozzi and Z.-L. Zhou, in Proc. of the 15^{th} Int. Conf. on Few-Body Prob. in Phys., Groningen, 1997 (to be published in Nucl. Phys. A).

[24] J.E. Ducret *et al.*, Phys. Rev. C **49**, 1783 (1994); Nucl. Phys. A **553**, 679c (1993); J.E. Ducret, Ph.D Thesis, Universite de Paris-Sud, Centre d'Orse (1992).

[25] D. Jordan, T. McIlvain *et al.*, Phys. Rev. Lett. **76**, 1579 (1996).

[26] K.F. von Reden *et al.*, Phys. Rev. C 41, 1084 (1990); R. Schiavilla *et al.*, Phys. Rev. C 40, 1484 (1989); G. Orlandini and M. Traini, Phys. Rev. C 31, 280 (1985); Z.E. Meziani *et al.*, Phys. Rev. Lett. 52, 2130 (1984); P. Barreau *et al.*, Nuovo Cim. 76 A, 361 (1983).

[27] TJNAF proposal E-94-004, "In-plane separations and high momentum structure function in $d(e,e'p)$ Reaction", P. Ulmer *et al.*, TJNAF PAC8 Report, 1994.

[28] M. van der Schaar *et al.*, Phys. Rev. Lett. **68**, 776 (1992).

[29] F. Frommberger *et al.*, Phys. Lett. B **339**, 17 (1994).

[30] H.J. Bulten *et al.*, Phys. Rev. Lett. **74**, 4775 (1995).

[31] W.-J. Kasdorp, Phys. Lett. B **393**, 42 (1997).

[32] J. Chen, X.Jiang, S.B. Soong, A. Young, and MIT-Bates OOPS Collab., preliminary data, 1997 (to be published).

[33] T. de Forest Jr., Nucl. Phys. A **392**, 232 (1983).

[34] M. Lacombe *et al.*, Phys. Rev. C **21**, 861 (1980).

[35] A. Pellegrino *et al.*, Phys. Rev. Lett. **78**, 4011 (1997).

[36] A proposal update for experiment 89-14 to the Bates 1997 PAC, W. Bertozzi, A.J. Sarty, L.B. Weinstein, and Z.-L. Zhou *et al.*, (1997).

[37] B.D. Milbrath, J.I. McIntyre *et al.*, submitted for publication (1997).

[38] D.H. Barkhuff, PhD thesis, University of Virginia, 1997 (unpublished).

[39] K. Joo, PhD thesis, MIT, 1997 (unpublished).

[40] TJNAF proposal E-89-028, "Polarization transfer measurements in the D$(\vec{e}, e'\vec{p})n$ Reaction", M. Finn and P. Ulmer *et al.*, TJNAF PAC4 Report, 1992.

[41] R.G. Arnold, C.E. Carlson and F. Gross, Phys. Rev. C **23**, 363 (1981).

[42] P.E. Ulmer, computer program MCEEP, TJNAF Tech. Note 91-101, (1991).

[43] J. Lightbody and J.S. O'Connell, Computers in Physics 2, 57 (1988).

[44] D.H. Barkhuff, private communication.

[45] K. Fissum *et al.*, "A study of the quasielastic $(e, e'p)$ reaction in ^{16}O at high recoil momentum, experiment handbook, V7.0, internal report #02/97 (unpublished).

[46] K. Wijesooriya, private communication.